Photon sensitive high index metal oxide films

2004 J. Phys.: Condens. Matter 16 S3757

(http://iopscience.iop.org/0953-8984/16/35/017)

INSTITUTE OF PHYSICS PUBLISHING JOURNAL OF PHYSICS: CONDENSED MATTER

J. Phys.: Condens. Matter **16** (2004) S3757–S3768 PII: S0953-8984(04)83262-4

Photon sensitive high index metal oxide films

G Kiriakidis[1] **and N Katsarakis**[1,2]

[1] Institute of Electronic Structure and Lasers (IESL), Foundation for Research and Technology Hellas (FORTH), PO Box 1527, 71110 Heraklion, Crete, Greece
[2] School of Applied Technology, Technological Educational Institute of Crete, PO Box 1939, 71004 Heraklion, Crete, Greece

Received 6 July 2004
Published 20 August 2004
Online at stacks.iop.org/JPhysCM/16/S3757
doi:10.1088/0953-8984/16/35/017

Abstract

In this work, we review the electrical and optical properties of InO_x and ZnO films, and their use as dynamic optical materials. The transport properties of these films are analysed and correlated with the growth parameters. We have studied the permanent light-induced refractive index changes in our dc-sputtered InO_x thin films using pulsed ultraviolet laser radiation at 193 nm. Non-permanent holography recording of information has been achieved in InO_x films upon illumination with UV radiation (325 nm). The recording, which appears to be independent of the electrical state of the material, disappears in the absence of UV light with decay times that depend on the material's specific properties, as these are influenced by the film fabrication conditions. We also review our work on waveguide reflection submicron relief gratings on multilayer waveguides operating near 1550 nm, fabricated by excimer laser ablation at 248 nm.

1. Introduction

Extended studies on transparent conducting oxide (TCO) nanocrystalline films, such as InO_x, ZnO, and In_2O_3: Sn (ITO), have been conducted due to the numerous potential technological applications. These oxides are known for their unique combination of optical and electrical properties. They present high transparency in the visible and near-infrared spectral region with relatively high conductivity, which allows them to be widely used as transparent conductors for devices such as electro-optic modulators, liquid crystal displays, and solar cells [1]. Furthermore, their relatively high refractive index ($n > 1.7$) [2] makes these films of interest as high refractive index overlayers for increasing the sensitivity of waveguides, while they may also be used as gas sensors and allow electrochemical control of sensing reactions [3].

Many different deposition techniques have been used to prepare thin TCO films. Some of the methods developed early on include spray pyrolysis [4–6], reactive evaporation [7], pulsed laser deposition (PLD) [8], the sol–gel method [9], and dc and rf sputtering [10]. These techniques with their associated processing parameters have an impact on the structural, optical, and

electrical properties of TCO films. Furthermore, the conductivity of polycrystalline InO_x, ZnO, and ITO films can be modified upon illumination with ultraviolet (UV) radiation ($h\nu > 3.5$ eV), resulting in a variable electrical state of the films from a resistive to a purely conductive one [11].

In this work, we review the electrical and optical properties of InO_x and ZnO films, and their use as dynamic optical materials. We have studied the permanent light-induced refractive index changes in our dc-sputtered InO_x thin films using pulsed ultraviolet laser radiation at 193 nm. Holography recording of information has been achieved in InO_x films upon illumination with UV radiation (325 nm). The recording, which appears to be independent of the electrical state of the material, disappears in the absence of UV light, with decay times that depend on the material's specific properties, as these are influenced by the film fabrication conditions. Moreover, research into photosensitive [12, 13] and relief [14, 15] gratings has been performed due to the interest in integrated optical devices and the research on alternative materials for telecommunications. In this respect, we also review earlier work on waveguide reflection submicron relief gratings on multilayer waveguides operating near 1550 nm, fabricated by excimer laser ablation at 248 nm.

2. Experimental details

Among the existing deposition techniques, magnetron sputtering was found to be the most widely used one for producing high quality TCO films with controlled properties. It provides good film uniformity, excellent adhesion, precise thickness control, surface smoothness, and less waste of expensive source material.

For producing our InO_x (ZnO) films, the depositions were carried out by dc magnetron sputtering in an Alcatel sputtering system with a 99.999% pure metallic indium (zinc) target (15 cm diameter) at a pressure of 8×10^{-3} mbar [16]. The base pressure of the chamber was 5×10^{-7} mbar. Corning 7059 glass substrates, which had thermally evaporated NiCr electrodes for electrical measurements, have been used. During the same run of deposition of films, different substrates with electrodes omitted were coated for performing the structural and morphological characterization of these films. In addition, the films were also deposited onto silica substrate for optical characterization. The substrate temperature was varied between room temperature (RT) and 400 °C, and the film thickness from 10 to 1100 nm. The stoichiometry of InO_x films was changed by altering the oxygen content of the sputtering atmosphere, and the potential of these thin films for novel chemical and optoelectronic applications has been investigated [17].

For the realization of holographic recording, a typical holographic set-up was used (figure 1). The beam of a HeCd laser emitting at $\lambda = 325$ nm was divided into two mutually coherent beams, by means of a dielectric beam splitter. The two beams, R_1 and R_2, with intensities of 300 mW cm^{-2} each, were subsequently directed onto the sample, forming an intensity interference pattern. Numerous recordings at various fringe spacing values (Λ) have been studied. A HeNe laser beam was used to monitor the recording of the holographic grating. The 5.7 mW HeNe probe beam, P, was incident normally onto the surface of the film. Two scattered beams of equal intensity, $S_{\pm 1}$, were observed corresponding to the ± 1 diffraction orders of the recorded sinusoidal grating. By using an optical powermeter and a storage oscilloscope, one of the two diffracted beams was monitored, in order to investigate the temporal characteristics of the recorded gratings.

3. Transport and optical properties

The electrical characterization was performed in a specially designed reactor described elsewhere [18]. The as-deposited films were all in an insulating state. For example, the

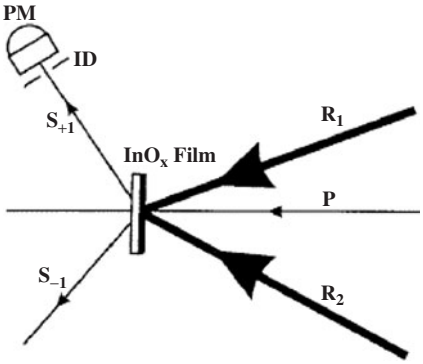

Figure 1. A schematic diagram of the experimental set-up used for holographic recording. R_1, R_2: recording beams at 325 nm; P: the HeNe probe beam at 633 nm; $S_{+1,-1}$: diffracted HeNe beams; PM: the powermeter head; ID: the iris diaphragm.

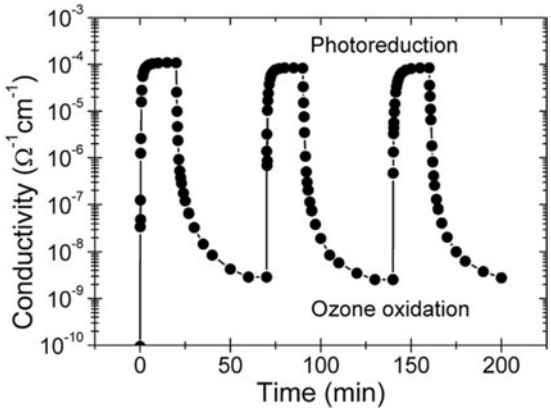

Figure 2. A typical photoreduction–oxidation cycle of a ZnO film.

as-deposited InO_x thin films showed a conductivity of less than $10^{-7}\ \Omega^{-1}\ cm^{-1}$ while for ZnO it was of the order of $10^{-10}\ \Omega^{-1}\ cm^{-1}$ in vacuum. For photoreduction the samples were directly irradiated in vacuum by the UV light of a mercury pencil lamp at a distance of approximately 3 cm for 20 min in order to achieve a steady state. For the subsequent oxidation the chamber was backfilled with oxygen at a pressure of 560 Torr and the samples were shielded from the lamp, which in this case served as a source for ozone production. This treatment lasted 40 min, after which no further changes of the conductivity could be observed. Finally, the chamber was evacuated and the photoreduction–oxidation cycle described above was repeated a few times. An electric field (1 or 10 V cm^{-1}) was applied during the whole cycling procedure to the samples and the electrical current was measured with an electrometer. The contact geometry for the two-probe measurement of the film's conductivity is described in detail in [17]. All conductivity measurements were carried out at room temperature. An I–V curve was recorded before the cycling started in order to ensure the Ohmic nature of the contacts. The photoreduction treatment results in an increase of the conductivity up to $10^{-4}\ \Omega^{-1}\ cm^{-1}$ for the ZnO films and 10^{-1}–$10^{-2}\ \Omega^{-1}\ cm^{-1}$ for the InO_x films, while conductivity values as low as $10^{-9}\ \Omega^{-1}\ cm^{-1}$ for ZnO and 10^{-3}–$10^{-6}\ \Omega^{-1}\ cm^{-1}$ for InO_x are obtained by subsequent ozone oxidation. This behaviour was completely reversible through many cycles of photoreduction and oxidation treatments, as shown for ZnO in figure 2.

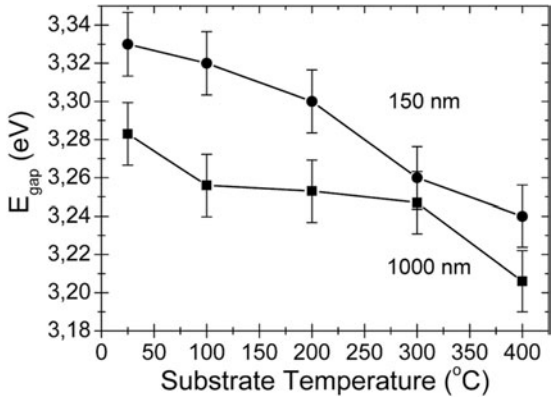

Figure 3. The dependence of the optical band gap for 150 nm (●) and 1000 nm (■) thick ZnO films on the substrate temperature during deposition.

The as-deposited InO_x and ZnO thin films were found to be highly transparent in the visible wavelength region with an average transmittance of 80% and showed an absorption edge in the UV depending slightly on deposition temperature. The optical energy gap E_{gap} was derived assuming a direct transition between the edges of the valence and the conduction band, for which the variation in the absorption coefficient with the photon energy $h\nu$ is given by

$$\alpha(h\nu) = A(h\nu - E_{\text{gap}})^{1/2}. \tag{1}$$

In equation (1), E_{gap} denotes the optical energy gap between the valence and the conduction band. By plotting α^2 versus $h\nu$ and extrapolating the linear region of the resulting curve, E_{gap} was obtained. A direct optical gap of 3.62 ± 0.05 eV was obtained for InO_x grown at room temperature. Similar results have been reported by Naseem *et al* [19] who measured energy gaps in the range from 3.67 to 3.92 eV for evaporated InO_x films, depending on the oxygen partial pressure during deposition. The calculated values of the direct optical energy gap varied between 3.21 and 3.33 eV for ZnO thin films depending on thickness and the substrate temperature during deposition. In figure 3, the dependence of the optical energy gap on the substrate temperature is depicted for 150 and 1000 nm thick ZnO films. It can be observed that the energy gap decreases with increasing substrate temperature, for both series of samples. Furthermore, the calculated energy gap for the thicker films is systematically smaller, which could be attributed to variations of the film density.

It has been suggested that two concurrent phenomena affect the optical band gap [20]. The first is the well-known Burstein–Moss shift (BM shift), which depends on the shape of the band edge and leads to an increase of the optical energy gap due to the filling of the lowest levels of the conduction band with charge carriers in degenerate semiconductors. The observed energy gap is then

$$E_{\text{gap}} = E_{\text{gap},0} + \Delta E_{\text{BM}}. \tag{2}$$

For parabolic band edges, ΔE_{BM} is given by

$$\Delta E_{\text{BM}} = \frac{\hbar}{2m^*_{vc}}(3\pi^2 n)^{2/3}. \tag{3}$$

The second phenomenon, which is responsible for the band gap shrinkage due to increased tailing of the absorption edge, is attributed to the merging of the donor states with the

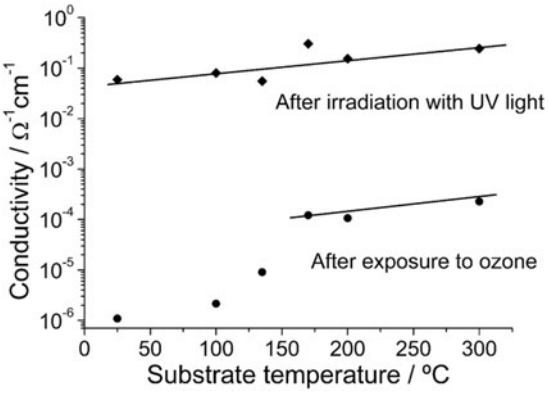

Figure 4. Maximum and minimum conductivities of InO_x films prepared at different substrate temperatures.

conduction band in the vicinity of the semiconductor–metal transition [21] and to electron–electron interactions [22]. The observation of a decreasing band gap with increasing substrate temperature leads to the assumption that the effect of band merging probably plays a dominant role in the films studied here, presumably caused by building up a donor band below the conduction band edge for films deposited at elevated temperatures. A detailed analysis of the transport properties, which is however beyond the scope of the work presented here, could provide further insight to the observed behaviour.

Regarding our analysis, in the following discussion the maximum conductivity (σ_{max}) denotes the conductivity in the conducting state of the sample after the irradiation procedure, while the minimum conductivity (σ_{min}) denotes the conductivity in the insulating state after re-oxidizing the sample.

At a fixed thickness of 150 nm, the substrate temperature during the deposition was varied between RT and 300 °C for InO_x and between RT and 400 °C for ZnO dc-sputtered thin films. All other deposition parameters were kept constant. The electrical measurements confirmed the strong change in the InO_x film properties around 170 °C (figure 4).

While the maximum conductivity was increasing only slightly with the deposition temperature from 5.5×10^{-2} to 3×10^{-1} Ω^{-1} cm^{-1}, the minimum conductivity showed very different behaviours for the low and high temperature growth regimes. Up to 170 °C the conductivity in the oxidized state increased more than two orders of magnitude, from 1.1×10^{-6} to 1.2×10^{-4} Ω^{-1} cm^{-1}, showing an intense thermally activated process which, besides the above band merging model, may also be related to inherent structural changes such as grain size increase [23]. Above 170 °C, the slight increase to 2.3×10^{-4} Ω^{-1} cm^{-1} followed qualitatively the behaviour of the maximum conductivity.

The influence of the film thickness on the electrical and structural properties of InO_x was investigated in the range from 10 to 1100 nm, comprising two orders of magnitude. The substrate temperature was set to 200 °C, which is above the crystallization temperature of amorphous InO_x films [24].

The film thickness mainly affected the maximum conductivity after irradiating the InO_x thin films with UV light (figure 5). The highest conductivity values were measured for the thinnest films. When the thickness of the films was increased by about two orders of magnitude, from 10 to 1100 nm, the maximum conductivity dropped by two orders of magnitude from approximately 100 to 1 Ω^{-1} cm^{-1}. The minimum conductivity, however, was almost constant in the region of 10^{-3} Ω^{-1} cm^{-1}.

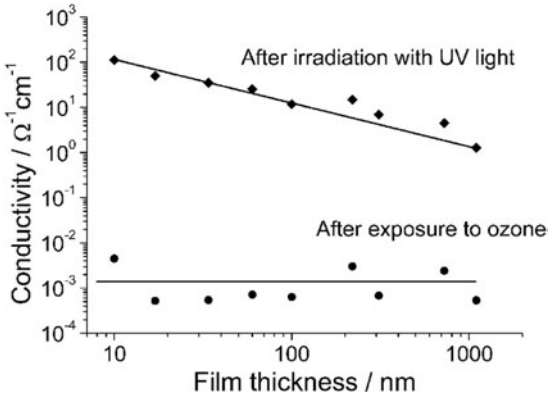

Figure 5. Maximum and minimum conductivities of InO_x films as a function of film thickness.

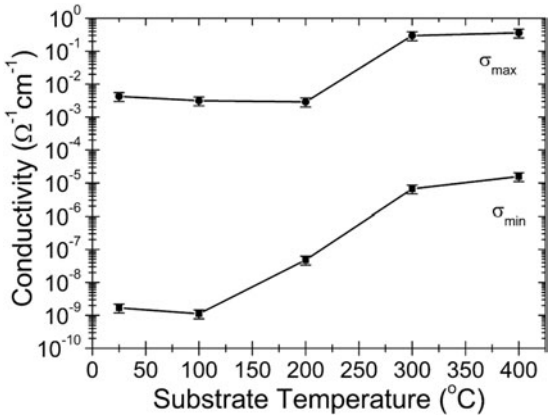

Figure 6. The dependence of the maximum conductivity after UV photoreduction (●) and the minimum conductivity after re-oxidation (■) on the deposition temperature of 150 nm thick ZnO films.

The electrical measurements for the ZnO film with a thickness of 150 nm are presented in figure 6. The maximum conductivity changed by about two orders of magnitude with increasing substrate temperature from RT to 400 °C. In detail, for $T < 200\,^{\circ}\mathrm{C}$, $\sigma_{\max}$ remained almost constant ($\sim 3 \times 10^{-3}\ \Omega^{-1}\ \mathrm{cm}^{-1}$), and then increased to $3 \times 10^{-1}\ \Omega^{-1}\ \mathrm{cm}^{-1}$ for $200\,^{\circ}\mathrm{C} < T \leqslant 400\,^{\circ}\mathrm{C}$.

The minimum conductivity, however, showed more pronounced changes and increased by four orders of magnitude between RT and 400 °C. For $T \leqslant 100\,^{\circ}\mathrm{C}$, $\sigma_{\min}$ remained almost constant ($\sim 2 \times 10^{-9}\ \Omega^{-1}\ \mathrm{cm}^{-1}$), while for $T \geqslant 200\,^{\circ}\mathrm{C}$ it increased abruptly, reaching a value of $\sim 10^{-5}\ \Omega^{-1}\ \mathrm{cm}^{-1}$ at 400 °C. The increase in $\sigma_{\min}$ with deposition temperature, as stated above, is probably due to an enhanced density of donor states, which are most probably forming a donor band just below the conduction band. The existence of such a donor band could explain the increase in $\sigma_{\min}$ as well as the observed decrease of the optical band gap with increasing substrate deposition temperature as discussed above. The step observed in $\sigma_{\min}$, $\sigma_{\max}$ versus substrate temperature curves in the range of $100\,^{\circ}\mathrm{C} < T < 200\,^{\circ}\mathrm{C}$ can also be related to the change in the preferred growth orientation in this temperature interval, as shown by XRD results [16, 25].

Table 1. The performance of the conductivities of some InO_x and doped In_2O_3 films with the corresponding operating temperatures.

Deposition technique	Substrate temperature	Conductivity (Ω^{-1} cm^{-1})	Reference
Sputtering	InO_x: RT	1.5×10^2	This work
	ZnO–InO_x: 350 °C	5×10^3	[26]
	ZnO–InO_x: RT	10^3	[26]
PLD	ITO: RT	2×10^2	[27]
Evaporation	InO_x: 0.5 °C s^{-1}	50	[28]
Spray pyrolysis	InO_x: 380 °C	7.8×10^2	[29]
	ITO: 350 °C	2×10^2	[29]

A number of groups have studied a wide range of TCO and their compounds prepared by sputtering, under different growth conditions [10, 25, 26]. Table 1 displays, in comparison with previous reports, the electrical properties of our sputtered InO_x films and those, including ZnO and ITO, prepared by PLD, spray pyrolysis, and evaporation techniques with the corresponding operating temperatures [26–29]. As can be seen, the electrical properties of TCO films are also dependent on the synthesis techniques used for their preparation. Our sputtered undoped InO_x films show good conductivity at RT, which is comparable only to the values found at higher temperatures by other techniques. This makes them very attractive for low temperature applications and thus opens new opportunities to use this material, in RT optoelectronic operations and as gas sensors, at ambient conditions without additional heating.

4. Photorefractive properties

On the basis of the above significant conductivity changes of these films, their photorefractive properties were explored by holographic recording experiments [30]. A very important characteristic of holograms is the diffraction efficiency, which is defined as the ratio of the light in the diffracted beam to the light flux in the incident beam (reading wave) that strikes the hologram. A typical sequence of holographic grating recording and decay in InO_x and ITO films has been observed and reported in [30]. It was established that the probe beam does not affect the recording characteristics that are solely associated with UV radiation.

Illumination with UV light in air increased the conductivity of an InO_x film by two orders of magnitude. An absolute change in the conductivity of InO_x with a thickness of $d = 270$ nm upon illumination with a HeCd laser beam of intensity $I = 2.8$ mW cm^{-2} was found. The new electrical state of the film was maintained until the film was exposed to an ozone atmosphere. Holographic recording was observed in both insulating and conducting states of the same film and the two recordings exhibit similar diffraction efficiency values. The above-mentioned experimental results suggested that optically induced conductivity changes were not responsible for holographic recording. If that were the case, then spatial modulation of conductivity would imply a permanent recording behaviour and different diffraction efficiency levels for specimens of differing conductivity. This was not observed here.

Furthermore, the hologram decay did not follow a simple exponential form. Double-exponential decay curves ($n = A_1 \exp(-t/\tau_1) + A_2 \exp(-t/\tau_2)$) fit well to the decay data (mean square error 10^{-5}) in [30]. Time constants $\tau_1 = 6.7$ s and $\tau_2 = 48$ s have been extracted from the fitting procedures. The decay time constants remained practically the same for all values of Λ in the range of 0.6–3 μm. A possible explanation of the origin of the observed behaviour was associated with involved active centres, such as oxygen vacancies, related to

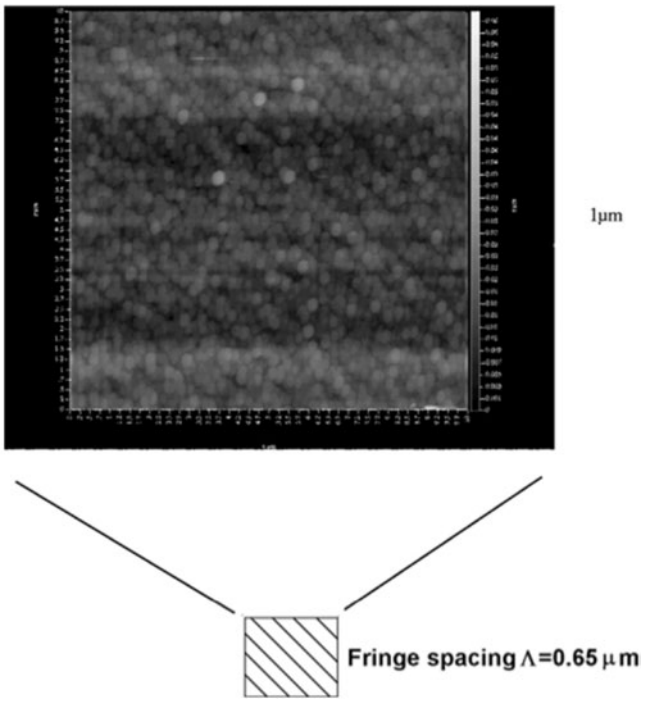

Figure 7. AFM scans of the illuminated area revealing a surface relief pattern of periodicity $\Lambda = 0.65\ \mu$m.

the growth conditions and the specific nature of the material. These localized states can be altered by UV radiation and their decay to the initial condition is associated with characteristic time constants that depend on the specific natures of the active centres and the material. This may also explain the difference in observed decay behaviour between gratings recorded for InO_x ($\tau_1 = 6.7$ s and $\tau_2 = 48$ s) and ITO ($\tau_1 = 14.5$ s and $\tau_2 = 138$ s). It was noted here that holographic recording measurements were performed with a large variety of specimens. Even though they were grown during different runs of the sputtering machine, they all exhibited identical temporal behaviour under the same experimental conditions.

We have also studied the permanent light-induced refractive index changes in our dc-sputtered InO_x thin films using pulsed ultraviolet laser radiation at 193 nm [31]. The photosensitivity of the films grown was investigated by exposing the samples to ultraviolet radiation from an injection-locked ArF excimer laser emitting coherent pulses of 23 ns duration with a mean energy of 100 mJ per pulse. The beam, after passing through a 50/50 dielectric beam splitter, was separated into two parts that were combined on the surface of the indium oxide film at a full crossing angle of $\sim 17^\circ$. The resultant interference pattern at this angle has a fringe spacing of 0.65 μm. Under pulsed exposure a grating was excited, which decayed initially, but finally stabilized at a steady-state value of diffraction efficiency, which was roughly half of the maximum. The dynamics of the recording and decay could be interpreted in terms of the coexistence of two different kinds of non-shifted gratings within the material. One grating corresponds to UV-induced electrical conductivity changes, which were observed earlier using longer wavelength exposure [30], whereas the second is a structural grating which remains after the thermal decay of the conductivity grating. This structural grating was revealed by atomic force microscope (AFM) scans performed on the UV-illuminated area. Figure 7 shows

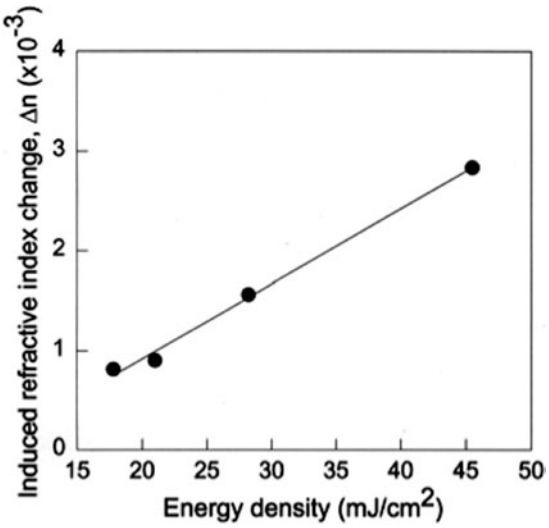

Figure 8. A plot of the magnitude of the photoinduced refractive index change as a function of the recording beam fluence.

the AFM scans that revealed a surface consisting of ∼300 nm size grains with imposed 650 nm periodic structures. Surface relief patterns are a common feature of photorefractivity in the UV region [32] indicating structural changes induced by the radiation.

The induced refractive index change, Δn, calculated from the diffraction efficiency using the thin grating diffraction formula [33] was plotted as a function of the excimer laser fluence per pulse and depicted in figure 8, showing the increase of the induced index change as a function of the laser fluence. It was difficult to specify the exact nature of the laser-induced structural modifications as they depended not only on the laser fluence and wavelength, but also on the precise growth conditions adopted for the films [31]. An increase of the magnitude of the index change was observed with increasing oxygen concentration in the sputtering chamber, which might well include a dependence on the sign of the change. This behaviour is common for other photosensitive materials such as germanium-doped silica [34] and lead germanate glasses [35].

We also review our work on waveguide reflection submicron relief gratings on multilayer waveguides operating near 1550 nm, fabricated by interferometer excimer laser ablation at 248 nm in collaboration with ORC of the University of Southampton [36]. The devices consisted of monomode potassium ion-exchanged channel waveguides in BK-7 glass overlaid for part of their length with a thin sputtered InO_x film in which the gratings were written, as shown in figure 9. The refractive index of the deposited layer ($n \sim 1.7$–1.8) is significantly higher than the maximum refractive index of the diffused channel waveguide, causing the optical field to be drawn up to the surface and interact strongly with the film [37]. The thickness of the overlayer was chosen so that it is below cut-off and, therefore, it does not itself form a waveguide in the wavelength region of interest. InO_x was chosen as it may be machined using low energy densities, avoiding damage to the underlying ion-exchanged region. Light from a single-mode telecommunication fibre, but coupled to the polished end face, excites the mode of the uncoated input section of the wavelength (A) and crosses the transition into the coated region (B). The modal intensity distribution in the coated region is drawn up to the surface by the high index film, as shown in figure 9, resulting in larger overlap and increased sensitivity to surface perturbations. The thickness of the overlayer was ideally chosen to be

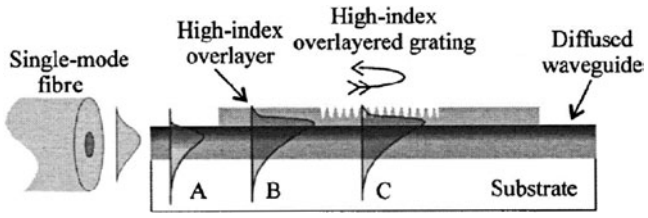

Figure 9. A schematic representation of a high index overlayer grating on an ion-exchanged waveguide: (A) the propagating mode in the uncoated region, (B) mode enhancement in the high index overlaid region, (C) interaction of the enhanced mode with the high index grating corrugation.

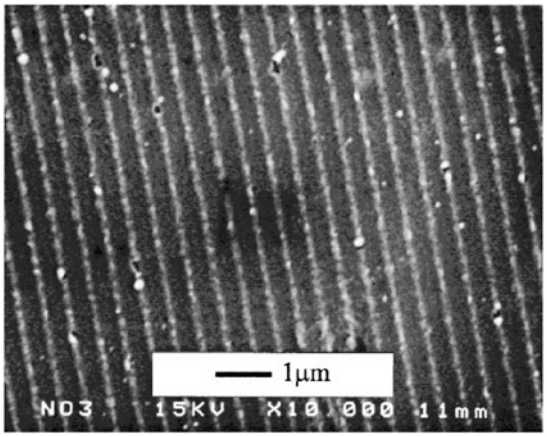

Figure 10. The grating ablated in a 100 nm thick InO_x film using 20 pulses of 45 mJ cm^{-2} energy density.

small enough that the coated waveguide is monomode and the scattering losses at the transitions are low. If a relief or photorefractive grating is recorded in the thin film overlayer (C), the field enhancement at the surface provides strong interaction of the guided field with the grating.

In more detail, waveguides were fabricated by ion exchange in two BK-7 glass substrates in molten potassium nitrate through aluminium mask openings ranging from 3 to 8 μm, at 400 °C for 11 h [36]. Polycrystalline indium oxide thin films, one of thickness 100 nm and one of thickness 135 nm, were sputtered on two waveguide chips using dc magnetron sputtering in a 100% O_2 atmosphere to cover a 25 mm length in the centre of the 40 mm long waveguides. The overlaid waveguides were exposed to a high contrast UV fringe pattern with a period of 514.3 nm using the three-mirror interferometer described elsewhere [38]. Gratings of 16 mm length were produced on each set of waveguides by exposure to an average pulse energy density of 45–60 mJ cm^{-2} using between 5 and 100 pulses. A scanning electron micrograph of a grating ablated in a 100 nm thick InO_x film using 20 pulses of energy density 45 mJ cm^{-2} is shown in figure 10. The transmission and reflection spectra for the TE polarization of an 8 μm wide channel waveguide overlaid with a 135 nm thick InO_x film supporting a grating ablated using five pulses of energy density 60 mJ cm^{-2} are shown in figure 11. The average grating depth was estimated to be approximately 20 nm from atomic force microscopy measurements. The transmission spectrum shows a broadband loss of about 4 dB, mainly due to fibre–waveguide coupling loss, including the transition losses between the coated and uncoated waveguide

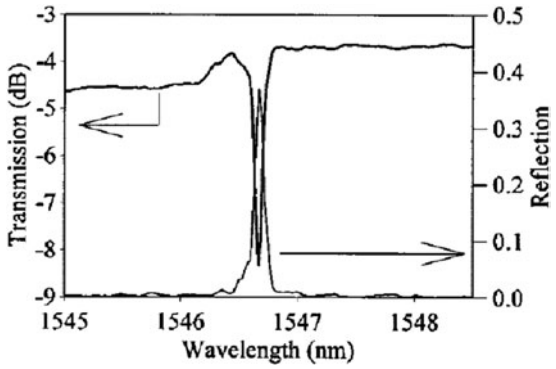

Figure 11. Transmission (thick curve) and reflection (thin curve) spectra for an 8 μm wide channel waveguide overlaid with a 135 nm thick InO_x film.

regions and propagation losses in the overlayer. The grating transmission showed a clear notch at 1456.7 nm with a depth of approximately 4.7 dB (66%) and a bandwidth at full width at half-maximum power ($\Delta\lambda_{FWHM}$) of 0.08 nm. At wavelengths shorter than the Bragg wavelength the transmission spectrum showed an increased broadband loss, which was attributed to coupling to radiation modes. The insertion loss of the waveguide overlayer clearly remained low even after UV exposure of the film. Exposures with higher energy densities or a large number of pulses resulted in significantly greater absorption loss and weaker grating strengths. Annealing of the waveguide chip up to 250 °C for 2 h in an oxygen atmosphere reduced the loss further by almost 1 dB. The reflection spectrum showed that reflected power was strongly coupled into the backward-travelling waveguide mode at 1546.7 nm. Due to the presence of the high index film on the waveguide surface, the electromagnetic boundary conditions yield much greater intensity at the surface of the indium oxide film for the TE than for the TM polarization [39]. In this case the grating coupling constant for the TM polarization was calculated to be 3.75 times smaller than for the TE polarization, resulting in a grating of predicted reflectivity no greater than 0.4 dB. Imperfections in the grating reduce the peak reflectivity further rendering this reflection immeasurable in comparison with spectral noise in the waveguide measurements.

5. Conclusions

Following a detailed study of parameters effecting conductivity changes, the holographic recording in InO_x transparent thin films has been studied at ultraviolet laser wavelengths. The observed holographic recording exhibits unusually large coupling strengths and a dynamic, yet slow, behaviour associated with the localized modification of the optical properties of the material. After the decay of the recorded grating, the material returned to its initial state. The observed behaviour was attributed to the existence of active centres in the materials. Permanent photorefractive recording in InO_x thin films using 193 nm excimer laser radiation was achieved. The dynamic characteristics of this recording and its dependence on the incident laser energy density and growth conditions were studied. The above data revealed the strong photorefractivity of InO_x induced by 193 nm pulsed radiation, and the dynamic behaviour of the material during and after recording. The feasibility of grating recording in InO_x with large values of refractive index change of $\sim 5 \times 10^{-3}$ using low energy fluence enables the use of InO_x as a photosensitive overlayer in telecommunications and sensor waveguide applications.

Acknowledgments

The authors of this review work would like to express their gratitude to a number of co-workers from FORTH and ORC of the University of Southampton who have collectively contributed to the study of these TCOs over the last few years.

The authors are grateful for support from the European Community's Human Potential Programme under contract HPRN-CT-2002-00298, RTN 'Photon-Mediated Phenomena in Semiconductor Nanostructures'.

References

[1] Granqvist C G 1993 *Appl. Phys.* A **57** 19
[2] Chen R T and Robinson D 1992 *Appl. Phys. Lett.* **60** 1541
[3] Luff B J, Wilkinson J and Perrone G 1997 *Appl. Opt.* **36** 7066
[4] Manifacier J C, Szepessy L, Bresse J F and Perotin M 1979 *Mater. Res. Bull.* **14** 163
[5] Siefert W 1984 *Thin Solid Films* **120** 275
[6] Bisht H, Eun H T, Mehrtens A and Aegerter M A 1999 *Thin Solid Films* **351** 109
[7] Penza M, Cozzi S, Tagliente M A, Mirenghi L, Martucci C and Quirini A 1999 *Thin Solid Films* **349** 71
[8] Adurodija F O 2002 *Handbook of Thin Film Materials* vol 1, ed H S Nalwa (San Diego, CA: Academic)
[9] Vaufrey D, Ben Khalifa M, Besland M P, Sandu C, Blanchin M G, Teodorescu V, Roger J A and Tardy J 2002 *Synth. Met.* **127** 207
[10] Vossen J L and Kern W 1991 *Thin Film Processes* vol 2 (New York: Academic)
[11] Fritzsche H, Pashmakov B and Claffin B 1994 *Sol. Energy Mater. Sol. Cells* **32** 383
[12] Geragthy D F, Provenzano D, Marshall W K, Honkanen S, Yariv A and Peyghambarian N 1999 *Electron. Lett.* **35** 585
[13] Ibsen M, Hubner J, Pedersen J E, Kromann R, Andersen L U A and Kristensen M 1996 *Electron. Lett.* **32** 2233
[14] Roman J E and Winick K A 1992 *Phys. Lett.* **61** 274417
[15] Adar R, Henry C H, Kistler R C and Kazarinov R F 1992 *Phys. Lett.* **60** 1779
[16] Kiriakidis G, Katsarakis N, Bender M, Gagaoudakis E and Cimalla V 2000 *Mater. Phys. Mech.* **1** 83
[17] Xirouchaki C 1998 *PhD Thesis* Crete p 58
[18] Xirouchaki C, Kiriakidis G, Pedersen T F and Fritzsche H 1996 *J. Appl. Phys.* **79** 9349
[19] Naseem S, Rauf I A and Hussain K 1988 *Thin Solid Films* **156** 161
[20] Hamberg I and Granqvist C G 1986 *J. Appl. Phys.* **60** R123
[21] Roth A, Webb J B and Williams D F 1982 *Phys. Rev.* B **25** 7836
[22] Gupta L, Mansingh A and Srivastava P K 1989 *Thin Solid Films* **176** 33
[23] Kiriakidis G 2003 *Int. Conf. on Nanomaterials and Nanotechnologies—NN2003l (Crete, Greece)* (Invited talk)
[24] Wyckoff R W G 1964 *Crystal Structures* (London: Wiley)
[25] Kiriakidis G, Bender M, Katsarakis N, Gagaoudakis E, Hourdakis E, Douloufakis E and Cimalla V 2001 *Phys. Status Solidi* a **185** 27
[26] Minami T, Kakumu T, Takeda Y and Takata S 1996 *Thin Solid Films* **290/291** 1
[27] Adurodija F O, Izumi H, Ishihara T, Yoshioka H and Motoyama M 2002 *Sol. Energy Mater. Sol. Cells* **71** 1
[28] Girtan M, Rusu G I, Rusu G G and Gurlui S 2000 *Appl. Surf. Sci.* **162/163** 492
[29] Prince J J, Ramamurthy S, Subramanian B, Sanjeeviraja C and Jayachandran M 2002 *J. Cryst. Growth* **240** 142
[30] Mailis S, Boutsikaris L, Vainos N A, Xirouchaki C, Vasiliou G, Garawal N, Kiriakidis G and Fritzsche H 1996 *Appl. Phys. Lett.* **69** 2459
[31] Pissadakis S, Mailis S, Reekie L, Wilkinson J S, Eason R W, Vainos N A, Moschovis K and Kiriakidis G 1999 *Appl. Phys.* A **69** 333
[32] Douay M, Xie X X, Taunay T, Bernage P, Niay P, Cordier P, Poumellec B, Dong L, Bayon J F, Poignant H and Delevaque E 1997 *J. Light-wave Technol.* **15** 1329
[33] Eichler H J, Gunter P and Pohl D W 1986 *Laser-Induced Dynamic Gratings* (Berlin: Springer)
[34] Bazylenko M V, Moss D and Canning J 1998 *Opt. Lett.* **23** 697
[35] Mailis S, Anderson A A, Barrington S J, Brocklesby W S, Greef R, Rutt H N, Eason R W, Vainos N A and Grivas C 1998 *Opt. Lett.* **23** 1751
[36] Pissadakis S, Reekie L, Zervas M N, Wilkinson J S and Kiriakidis G 2001 *Appl. Phys. Lett.* **78** 694
[37] Quigley G R, Harris R D and Wilkinson J S 1999 *Appl. Opt.* **38** 6036
[38] Pissadakis S, Reekie L, Hempstead M, Zervas M N and Wilkinson J S 2000 *Appl. Surf. Sci.* **153** 200
[39] Quigley G R, Harris R D and Wilkinson J S 1999 *Appl. Opt.* **38** 6036